SSIM 2025 - JJ Potter & J Wesseloo (eds)

doi:10.36487/ACG_repo/2535_0.02

Leps 2.0: updated strength envelopes for rockfill based on 900 large-scale triaxial tests

Scott D Cylwik [a,*], Marco Arrieta [b], John C Cunning [c], P Mark Hawley [d]

[a] *Call & Nicholas, Inc, USA*

[b] *University of Oulu, Finland*

[c] *WSP, UK*

[d] *Piteau Associates, Canada*

Abstract

This paper presents a new shear strength criterion and empirical model for rockfill and coarse mine waste rock. The model is supported by a database of over 900 large-scale triaxial tests and is intended to update and improve upon the Leps strength envelopes commonly used for rockfill materials. The nonlinear shear strength criterion uses a single physically based input parameter, can reproduce the Leps strength envelopes, transitions smoothly between strength categories, and is compatible with both shear/normal and principal stress data. An empirical model is also presented to rapidly estimate rockfill strength from void ratio and rock type, providing a practical tool for field application when laboratory testing is unavailable. The model simplifies into five strength categories and maintains predictive accuracy with minimal complexity. Statistical analysis suggests that the models are applicable for materials with a median particle size greater than 2 mm and a fines content less than 25%. Two cases are presented that demonstrate practical application of the model for a rockfill dam and a mine waste stockpile.

Keywords: *rockfill, shear strength, large-scale triaxial tests, waste dumps, heap leach pads*

1 Introduction

Rockfill is an important construction material in both mining and civil engineering, commonly used to construct large embankments, dams and waste rock storage facilities (Leps 1988). In open pit mining, rockfill is used to construct waste dumps and heap leach pads that may reach several hundred metres in height (Valenzuela et al. 2008). Figure 1 presents a schematic cross-section through a waste dump at a large open pit mine, highlighting some of the geotechnical challenges related to their operation, characterisation, analysis and management. The stability and performance of these structures rely heavily on the shear strength of rockfill, a property that depends on several factors including confining stress, particle size, particle shape, particle strength and degree of compaction.

In the mining environment, rockfill is typically produced by blasting and often contains particles too large for conventional laboratory testing, making direct strength estimation from standard tests challenging. Additional complications arise from scale effects and the inherently nonlinear behaviour of coarse, angular materials (Xiao et al. 2016; Ovalle et al. 2020). For decades, practitioners have used the Leps (1970) strength envelopes successfully as a baseline for estimating rockfill strength, particularly in the absence of site-specific test data. Although these envelopes have been widely applied in major civil and mining projects (Hawley & Cunning 2017), they were developed from a limited dataset and lack a systematic approach for assigning materials to a strength category.

[*] Corresponding author. Email address: scylwik@cnitucson.com

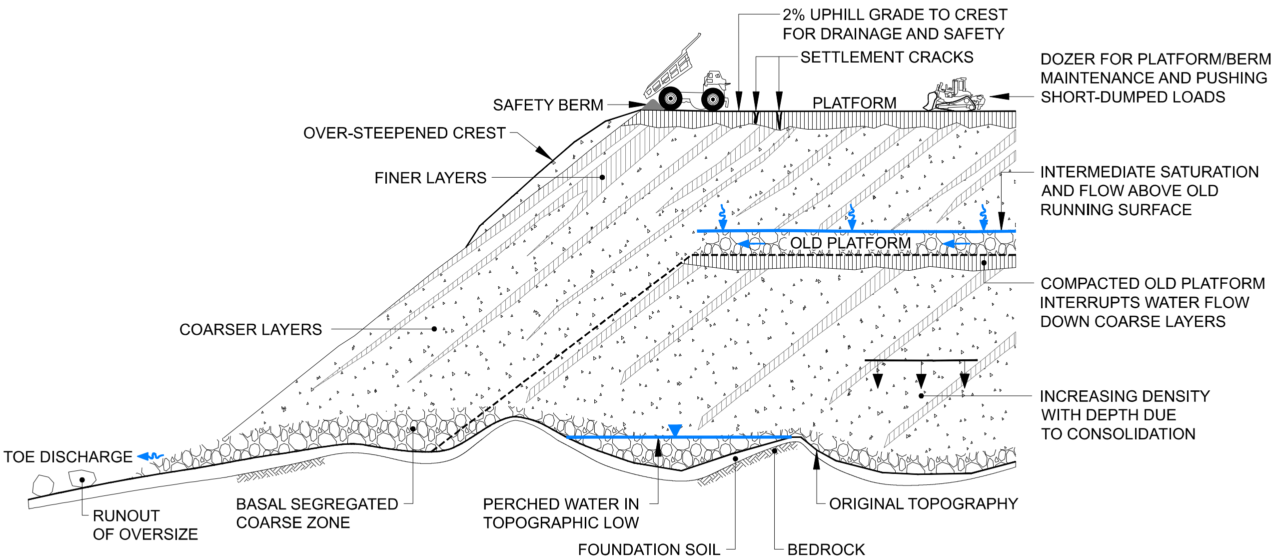

Figure 1 Schematic cross-section of a large waste dump at an open pit mine

To address these limitations, this paper presents a new strength criterion and empirical model that was developed and calibrated using a database of over 900 large-scale triaxial tests. The proposed model captures the nonlinear strength behaviour of rockfill through a single, physically meaningful parameter and is designed to be practical for use in both laboratory analysis and field applications. The criterion enables smooth transitions between strength categories and can be interpreted using either shear/normal or principal stress data. The methodology and model development are summarised from Cylwik et al. (2025), with new examples included here to illustrate practical applications such as strength increases due to consolidation of waste dumps and strength decreases due to weathering of rockfill.

2 Laboratory testing database

The database consists of 934 large-scale triaxial tests conducted on rockfill materials with measurement of effective stress parameters, in addition to four large-scale direct shear tests. It is an extension of the database originally compiled by Douglas (2002) and draws from 41 published sources. The complete dataset is available for download from an online repository (Arrieta 2025).

To estimate effective normal stress (σ_n) and shear stress (τ) for each triaxial test, the iterative procedure outlined by Cylwik et al. 2025 was used. This approach accounts for the nonlinearity of the failure envelope, since σ_n and τ are not directly measured from a triaxial test but must be estimated from a set of major (σ_1) and minor (σ_3) principal effective stresses at failure (Baker 2004). Other important characteristics of the database include:

- The rockfill samples tested span a broad range of particle sizes, with median particle sizes (D_{50}) up to 100 mm (Figure 2a).
- The maximum particle sizes (D_{max}) tested ranged from 4.8 to 200 mm.
- The average triaxial cell diameter (D_S) was 396 mm, with a maximum of 1,130 mm (Figure 2b).
- The average gravel content of the samples was 78%, with little to no fines. Only 10% of the samples had a fines content greater than 20%.
- The uniaxial compressive strength of the particles ranged from 25 to 300 MPa; rockfill composed of weak rock was not considered in this study.
- Tests lacking reported rock type or initial void ratio (e) were omitted as these parameters are required for the proposed empirical model.

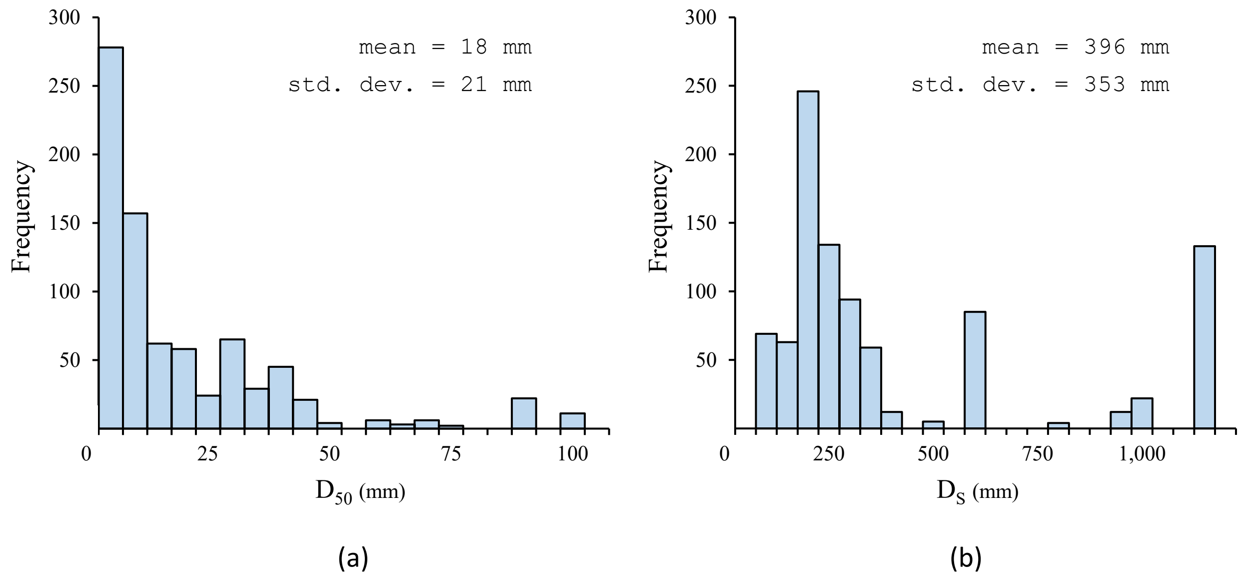

Figure 2 Distribution of samples in the rockfill database. (a) Median particle size; (b) Test cell diameter

The secant friction angle ($\emptyset'_S$) was calculated for each test in the database using Equation 1. This angle represents the slope of the line connecting the origin to a point on the failure envelope in shear/normal stress space. Figure 3 presents a plot of secant friction angle versus the logarithm of normal stress for all 938 tests in the database, grouped by similar rock types. This type of chart mirrors the one originally used by Leps (1970) to assess typical ranges of rockfill shear strength.

The downward trend observed in Figure 3 confirms the nonlinear nature of the rockfill failure envelope, consistent with previous findings of other researchers (e.g. Charles & Watts 1980; Indraratna et al. 1998; Xiao et al. 2016; Ovalle et al. 2020). In a linear Mohr–Coulomb model, the secant friction angle would remain constant and the data in Figure 3 would form a horizontal line. Instead, the observed decrease in secant friction angle with increasing normal stress reflects the stress-dependent behaviour of rockfill.

This nonlinearity is primarily driven by the suppression of dilation at higher stress levels. At low confining stresses, interlocked particles undergo significant dilation, resulting in high secant friction angles (Ladanyi & Archambault 1969; Bahrani & Kaiser 2020). As normal stress increases, dilation is gradually reduced, and shear strength is instead mobilised through asperity shearing and particle crushing (Barton 2016).

$$\emptyset'_S = \operatorname{atan}\left(\frac{\tau}{\sigma_n}\right) \tag{1}$$

where:

$\emptyset'_S$ = secant friction angle

τ = shear stress at failure

σ_n = effective normal stress at failure.

3 Failure criterion

For a soil in direct shear, the basic form of the failure criterion is shown in Equation 2. The criterion follows a standard cohesionless power-law form, except that it is normalised by the standard atmospheric pressure constant (p_a). This normalisation makes the strength coefficient (K) unitless and invariant for any system of units. The curvature coefficient (m) controls the nonlinearity of the failure envelope. According to Mohr failure theory, m is restricted to between 0.5 and 1.0 (Anyaegbunam 2015; Yu et al. 2020) for a cohesionless power curve, with m = 1 resulting in a linear Mohr–Coulomb envelope.

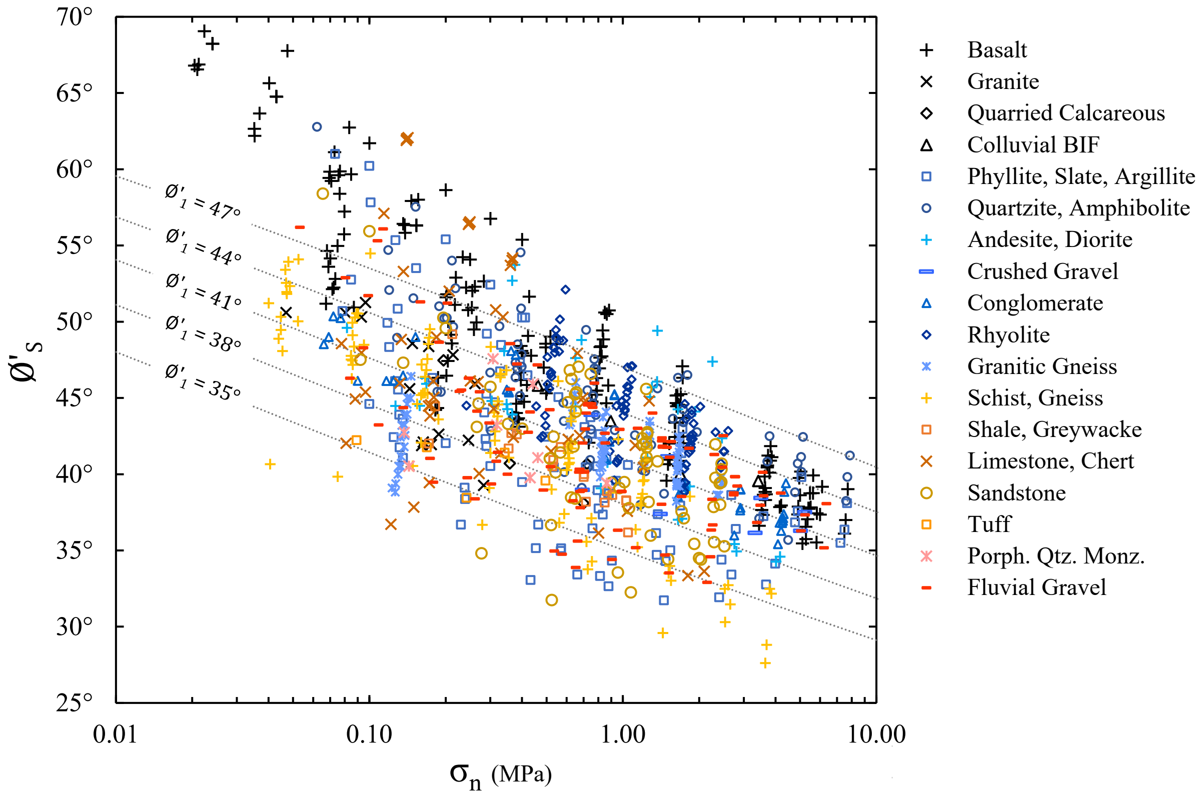

Figure 3 **Normal stress versus secant friction angle, sorted by rock type (938 tests)**

$$\tau = K p_a \left(\frac{\sigma_n}{p_a}\right)^m \tag{2}$$

where:

K	=	strength coefficient (dimensionless)
m	=	curvature coefficient (dimensionless)
p_a	=	standard atmospheric pressure = 101.3 kPa = 14.70 psi = 2,116 psf.

To express the failure criterion in a practical form, the parameter K was redefined in terms of a secant friction angle. This was achieved by setting $\sigma_n = 10\,p_a$ and $\tau = 10\,p_a \tan\emptyset_1'$ in Equation 2, solving for K, and substituting this value to yield Equation 3. In this formulation, $\emptyset_1'$ represents the secant friction angle at a normal stress of $10\,p_a$ (approximately 1 MPa). This stress level is referred to as the anchor stress, since the strength (and secant friction angle) will be constant at that point for any value of m. This concept is illustrated in Figure 4a, which shows example strength envelopes generated with Equation 3.

$$\tau = \tan\emptyset_1' \,(10\,p_a)^{1-m}\,{\sigma_n}^m \tag{3}$$

where $\emptyset_1'$ is the secant friction angle at σ_n = 10 p_a.

A typical value for the curvature coefficient m of rockfill is 0.9 although it may range from 0.80 to 0.95, depending on the characteristics of the material, testing methods and sample preparation procedures (Douglas 2002; Cylwik et al. 2023, 2025). Assuming the typical value of m = 0.9, the failure criterion simplifies to Equation 4.

$$\tau = \tan\emptyset_1' \,(10\,p_a)^{0.1}\,{\sigma_n}^{0.9} \tag{4}$$

Equations 3 and 4 offer several advantages for modelling the strength of rockfill:

- Reproduction of established envelopes. Equation 4 can replicate many well-known failure envelopes for rockfill, including the Leps (1970) envelopes, those from the Large Open Pit Project Guidelines for Mine Waste Dump and Stockpile Design (Hawley and Cunning 2017), and the lower-bound envelope of Indraratna et al. (1993). The corresponding $\emptyset_1'$ values to create each envelope are summarised in Table 1, and the Leps envelopes are shown in Figure 4b.

- Physically meaningful, intuitive input parameter. The fitting parameter $\emptyset_1'$ represents a secant friction angle expressed in degrees, providing a direct physical meaning that makes it easier to communicate, interpret and compare nonlinear rockfill strengths.

- Smooth strength transitions. The criteria allow for continuous, realistic transitions between different strength categories.

- No unit conversion complications. The formulation reduces the risk of unit conversion mistakes that can occur with power-law failure criteria, since the input parameter is expressed in degrees and applies consistently across unit systems.

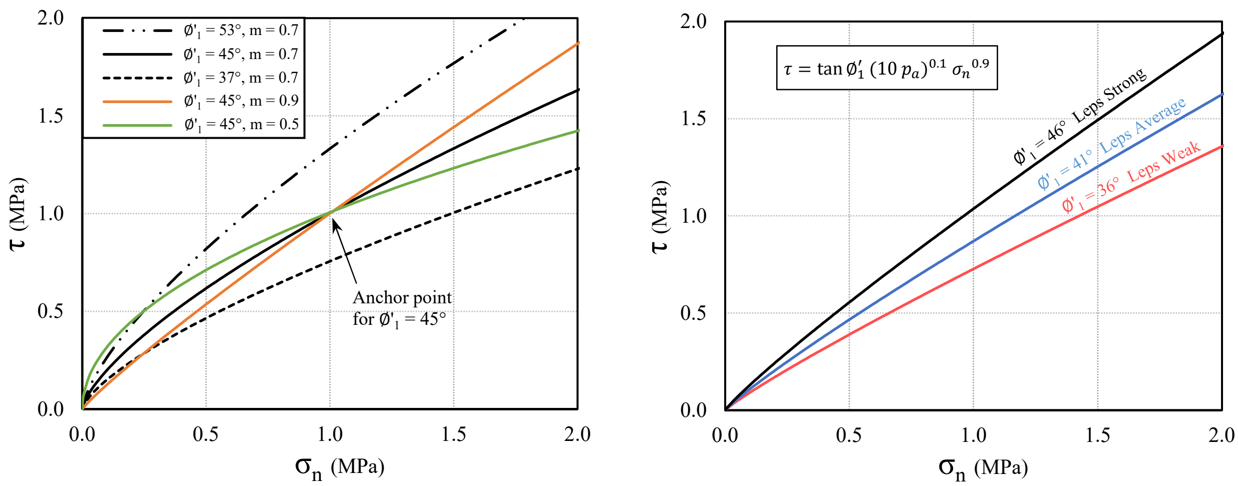

(a) (b)

Figure 4 **Strength envelopes with the nonlinear criterion. (a) Sensitivity to $\emptyset_1'$ and m; (b) Recreation of the Leps strength envelopes**

Table 1 **Established strength envelopes for rockfill that are reproduced by the criterion ($m = 0.9$)**

$\emptyset_1'$	Leps (1970) rockfill	Hawley & Cunning (2017) rockfill	Indraratna et al. (1993) rockfill
33°	–	–	Lower limit strength
36°	Weak/loose/poorly graded	Top-down construction, very high to high hazard	–
38°	–	Top-down construction, moderate to low hazard	–
41°	Average	–	–
43°	–	Bottom-up construction, very high to high hazard	–
46°	Strong/dense/well graded	Bottom-up construction, moderate to low hazard	–

3.1 Principal stress

Stress pairs can be converted to the effective principal stresses at failure using Equations 5 to 7, which have been derived from the solutions presented in Balmer (1952) (Cylwik et al. 2024). These equations enable the generation of failure envelopes in terms of σ_1 and σ_3.

$$\sigma_1 = \sigma_n + \tau \tan\beta \tag{5}$$

$$\sigma_3 = \sigma_n - \frac{\tau}{\tan\beta} \tag{6}$$

$$\beta = \frac{\varphi}{2} + \frac{\pi}{4} = \frac{1}{2}\operatorname{atan}\left(\frac{d\tau}{d\sigma_n}\right) + \frac{\pi}{4} = \frac{1}{2}\operatorname{atan}\left(\tan\emptyset_1' \times 10^{1-m}\, m\left(\frac{\sigma_n}{p_a}\right)^{m-1}\right) + \frac{\pi}{4} \tag{7}$$

where:

σ_1 = major principal effective stress at failure

σ_3 = minor principal effective stress at failure

β = angle of failure plane with respect to σ_3.

The failure criterion can be expressed directly in terms of principal stresses and the instantaneous friction angle (φ), as shown in Equation 8. The derivation of this equation is outlined in Cylwik et al. (2025).

$$\sigma_1 = \sigma_3 + \sigma_3 \frac{2\sin\varphi}{(1-m)\sin^2\varphi - \sin\varphi + m} \tag{8}$$

While it is not possible to directly derive the failure criterion solely in terms of principal stresses, an approximation has been developed to aid practitioners when an explicit closed-form solution is required. Equation 9 may be combined with Equation 8 to estimate the failure stress with less than 1% error subject to the conditions of 0.7 < m < 1 and 25˚ < $\emptyset_1'$ < 50˚.

$$\tan\varphi \approx (\tan\emptyset_1' \times 10^{1-m}\,(1.714m - 0.714) - 0.289\ln(m) - 0.007)\left(\frac{\sigma_3}{p_a}\right)^{(0.528m^2+0.0021m-0.528)} \tag{9}$$

4 Empirical model

To evaluate which parameters exert the strongest influence on the shear resistance of rockfill, the measured strength values were compared to various sample characteristics recorded in the database, such as gravel content, particle size and particle strength. The most consistent correlations were obtained when:

- The samples were grouped by both initial void ratio (e) and rock type.
- The database was analysed by test set rather than by individual test. A regression was fit to estimate $\emptyset_1'$ and m using Equation 3 for each set of tests performed on the same material at different confining pressures (249 total test sets in the database from the 938 tests).

Two clear trends emerged from the analysis: lower void ratios correlated with higher shear strengths, and certain rock types consistently exhibited greater strength. Based on these observations, the rock types in the database were sorted into three quality categories according to their measured strength: good, moderate and low, as summarised in Table 2. An example of these correlations is shown in Figure 5a, illustrating the clear trend of decreasing strength with increasing void ratio for rock types classified as good quality. These rock type quality groupings reflect strength trends observed in the database and are intended as screening guidance rather than a substitute for site-specific strength characterisation.

To capture these relationships quantitatively, a simple model was developed to relate the secant friction angle to void ratio and rock type, as presented in Equation 10. Combining Table 2 with Equations 4 and 10 to predict the shear strength of every test in the database yielded an R^2 coefficient of 0.991 and an average absolute relative error percentage of 10.5%, as shown in Figure 5b.

$$\varnothing'_1 = \varnothing'_{e=0} - \omega \times e \approx \varnothing'_{e=0} - 20° \times e \quad (10)$$

where:

$\varnothing'_{e=0}$ = secant friction angle intercept at a theoretical void ratio of zero

ω = slope parameter on a plot of e versus $\varnothing'_1$

e = void ratio

$\varnothing'_{e=0}$ ≈ 53° for good quality rockfill

$\varnothing'_{e=0}$ ≈ 50° for moderate quality rockfill

$\varnothing'_{e=0}$ ≈ 47° for low quality rockfill.

Table 2 Rock types in the database sorted into each rockfill quality category

Good	Moderate	Low
Basalt	Phyllite	Gravel
Latite basalt	Slate	Clayey gravel
Dolomitic basalt	Andesite	Gravelly sand
Granite	Argillite	Gneiss
Quarried calcareous	Quartzite	Limestone
Colluvial banded iron formation	Crushed gravel	Sandstone
–	Diorite	Siltstone
–	Conglomerate	Schist
–	Silicified conglomerate	Shale
–	Amphibolite	Greywacke
–	Granitic gneiss	Tuff
–	Rhyolite	Argillaceous chert
–	–	Porphyritic quartz monzonite

Table 3 Predicted $\varnothing'_1$ by rockfill quality and compaction with the empirical model

	Compaction		
Rockfill quality	Dense e = 0.3	Medium e = 0.45	Loose e = 0.6
Good	47°	44°	41°
Moderate	44°	41°	38°
Low	41°	38°	35°

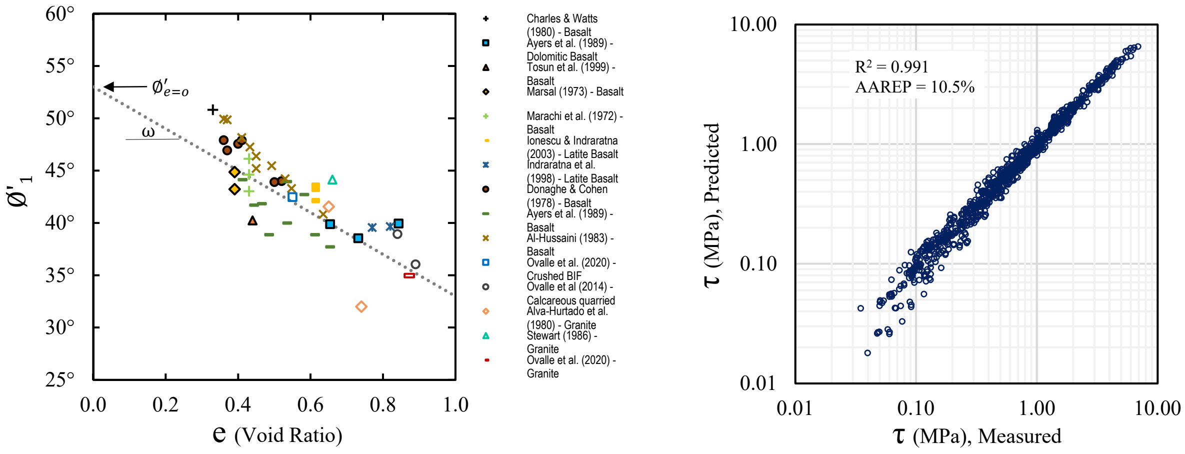

(a) (b)

Figure 5 **(a) Measured $\emptyset_1'$ for test sets on rock types classified as high quality; (b) Measured shear strength versus predicted shear strength with the proposed models (average absolute relative error percentage [AAERP])**

While rock type can typically be assessed easily in the field, the in situ void ratio will not always be available or readily obtainable. In these situations, the empirical model can be simplified into three compaction categories – dense, medium and loose – based on typical void ratio ranges for rockfill. Combining these three compaction levels with the three rock type quality categories produces five unique strength envelopes when Equation 10 is applied, corresponding to $\emptyset_1'$ values of 47, 44, 41, 38 and 35°. These categories are summarised in Table 3 and offer a practical, rapid method for estimating rockfill strength when limited data are available. Although the model provides useful guidance, site-specific testing remains essential for high-consequence or critical design applications.

4.1 Visual evaluation of model accuracy

The accuracy of the model predictions for all tests in the database are illustrated in Figures 6 and 7, which plot the normalised secant friction angle and shear stress for different rock type quality and compaction categories. Because tests performed at different void ratios are not directly comparable, the measured strength values were normalised to the void ratios in Table 3 for each category using the procedure described by Cylwik et al. (2025) to enable direct comparison across tests.

The data were sorted into the nine categories listed in Table 3, with the predicted strength envelopes from Equation 4 for each category also shown for reference (perfect model predictions would plot on these envelopes). Figures 6 and 7 demonstrate the grouping of shear strength by void ratio and rock type, highlighting the model's predictive capability. These plots also provide a visual indication of the expected variability and accuracy when applying the model across different compaction levels and stress conditions.

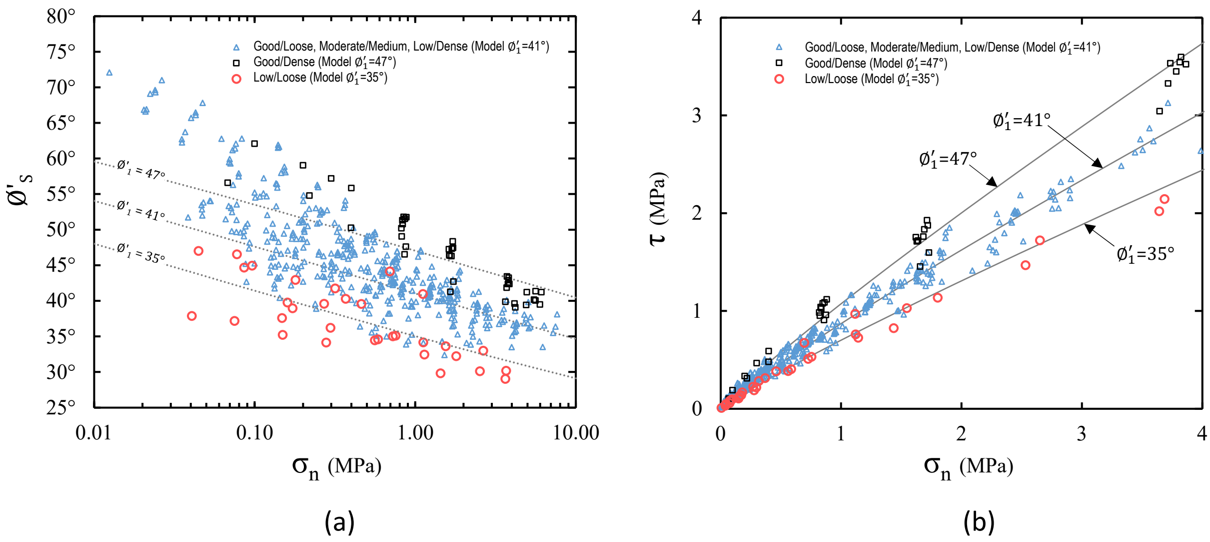

Figure 6 Normalised (a) secant friction angle and (b) shear strength, for good rock type quality (dense and loose), moderate rock type quality (medium) and low rock type quality (dense and loose)

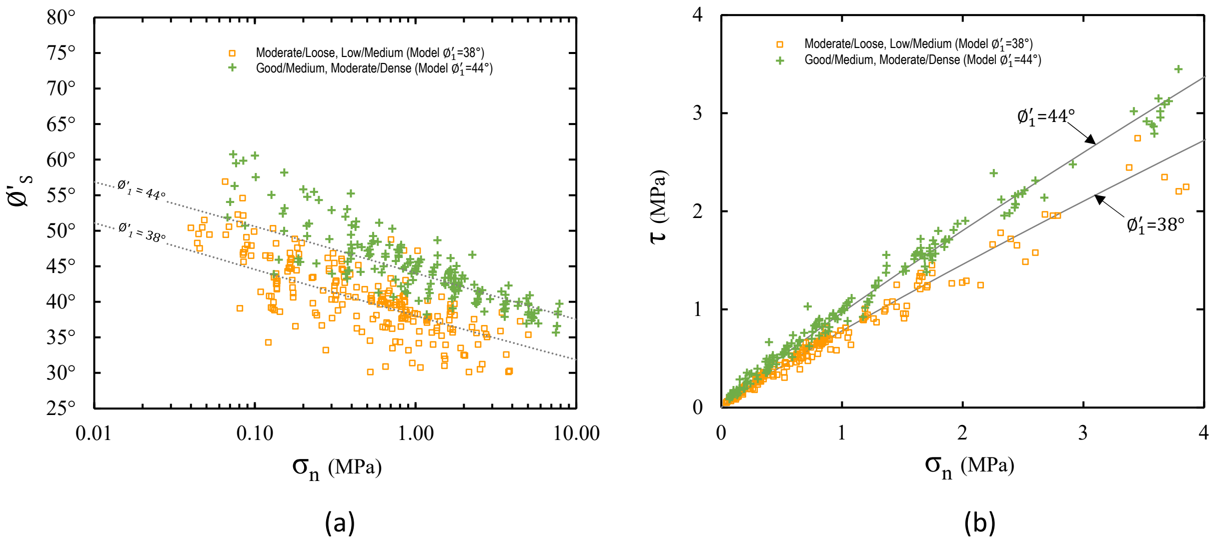

Figure 7 Normalised (a) secant friction angle and (b) shear strength, for good rock type quality (medium), moderate rock type quality (loose and dense) and low rock type quality (medium)

4.2 Model application range

Residual model error was evaluated for each test to determine the valid range of model application. The model, on average, produces reasonable predictions when D_{50} > 2 mm and shows no consistent trend with respect to D_{max}. However, performance declines in soils with less than 50% gravel and more than 10% fines – especially when fines exceed 30%, where the model tends to overestimate strength. These trends are consistent with transitions in mechanical behaviour observed in controlled soil mixing tests (Park & Santamarina 2017). Based on these findings, the model is expected to perform adequately for granular materials with > 40% gravel (D_{50} > 2mm) and < 25% fines, as illustrated in Figure 8. Materials with gradation curves that fall entirely within the green zone in Figure 8 are anticipated to exhibit rockfill mechanical behaviour. Park & Santamarina noted that the boundary locations in Figure 8 can shift depending on additional factors, such as the plasticity of the fines and the angularity of the coarse particles. For example, higher plasticity fines may cause the boundary to shift downward, whereas more rounded particles may cause it to shift leftward. Site-specific characterisation is advised for materials on or near the boundaries.

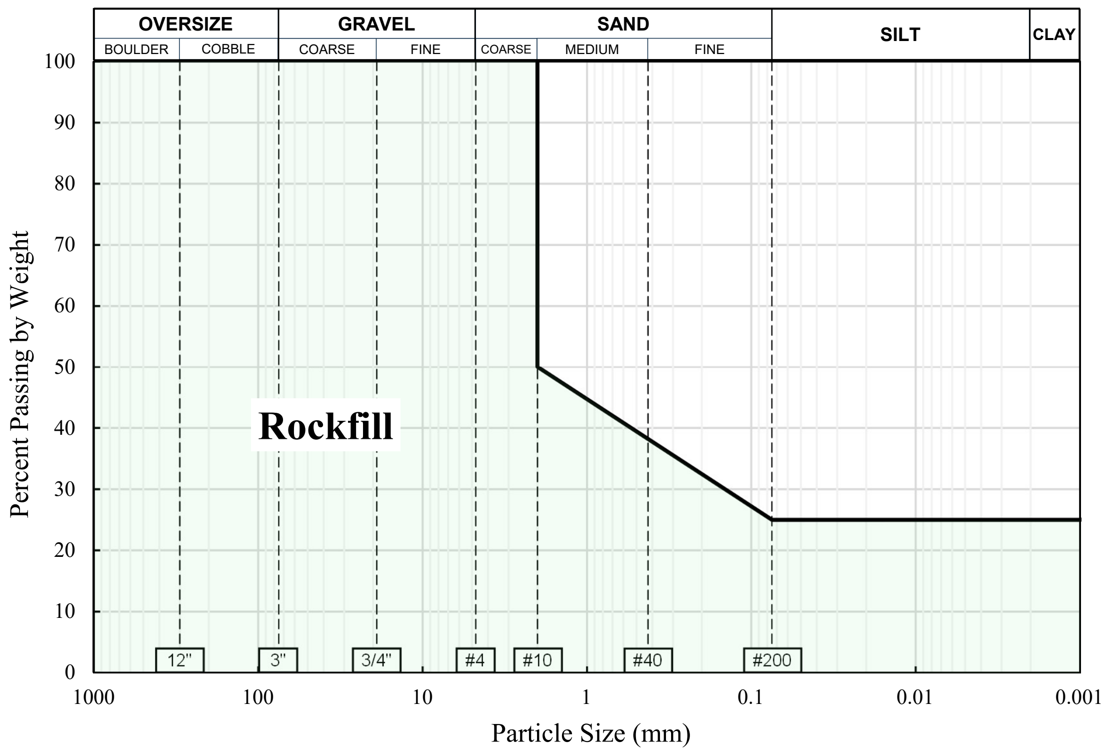

Figure 8 **Proposed zone defining rockfill mechanical response on the particle size distribution plot**

4.3 Testing guideline

The proposed model consistently underestimates rockfill strength at stress levels below σ_n = 100 kPa (Figures 6a and 7a), suggesting that if tests below this level are used for model calibration, strengths could be overestimated or underestimated for σ_n > 100 kPa. To address this potential issue, the testing guidance outlined in Table 4 is reccommended when calibrating a power-law failure criterion for rockfill. Adhering to this guidance should improve the accuracy of strength estimates at higher stress levels (σ_n > 100 kPa), but may produce conservative estimates of strength at lower stress levels.

Table 4 **Summary of the '60–600 Guideline' for rockfill (adapted from Cylwik et al. 2025)**

Recommendation	Triaxial σ_3 (kPa)	Direct shear σ_n (kPa)
Avoid using tests below this stress level when calibrating a power-law failure criterion	60	100
Incorporate at least one test above this stress level when calibrating a power-law failure criterion	600	1,000

5 Example applications

5.1 Weathering of rockfill

Basalt riprap rockfill used to construct the upstream slope of the Marimbondo Dam in Brazil has shown signs of degradation due to natural weathering processes. To investigate long-term behaviour of this basalt rockfill, Sayão et al. (2005) created artifically weathered/altered samples in the laboratory by using the continuous lixiviation technique with a Soxhlet apparatus for 430 hours. This accelerated weathering process resulted in mineral dissolution, hydrolysis, breakdown of mafic minerals, leaching of oxides and propagation of fissures. Images of the basalt rockfill in the field and after weathering are shown in Figure 9.

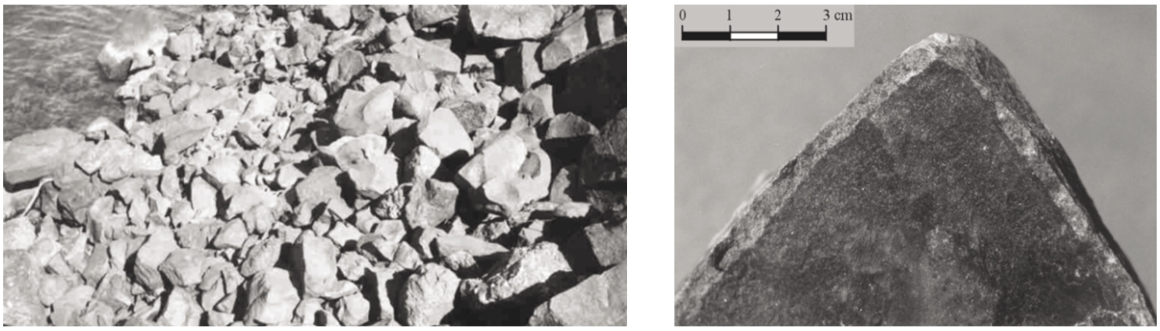

(a) (b)

Figure 9 (a) Upstream protection rockfill at Marimbondo Dam; (b) observed weathering of basalt rockfill particle at Marimbondo (images adapted from Sayão et al. [2005], licensed under CC BY-NC)

Sayão et al. (2005) conducted large-scale direct shear tests using a 1 m shear box on both loose and compacted samples, with relative densities (D_r) of 30% and 90%, respectively, under both dry and submerged conditions. The tested basalt rockfill samples had the following characteristics: D_{50} = 100 mm and D_{max} = 140 mm, C_u = 2.6 (uniformity coefficient), and estimated void ratios of e = 0.33 and e = 0.53 for the dense and loose samples, respectively. The test results, shown in Figure 10, clearly indicated that shear strength decreased with greater degrees of weathering and increased with compaction. No significant difference in shear strength was observed between the dry and submerged tests, and therefore these results were combined for analysis.

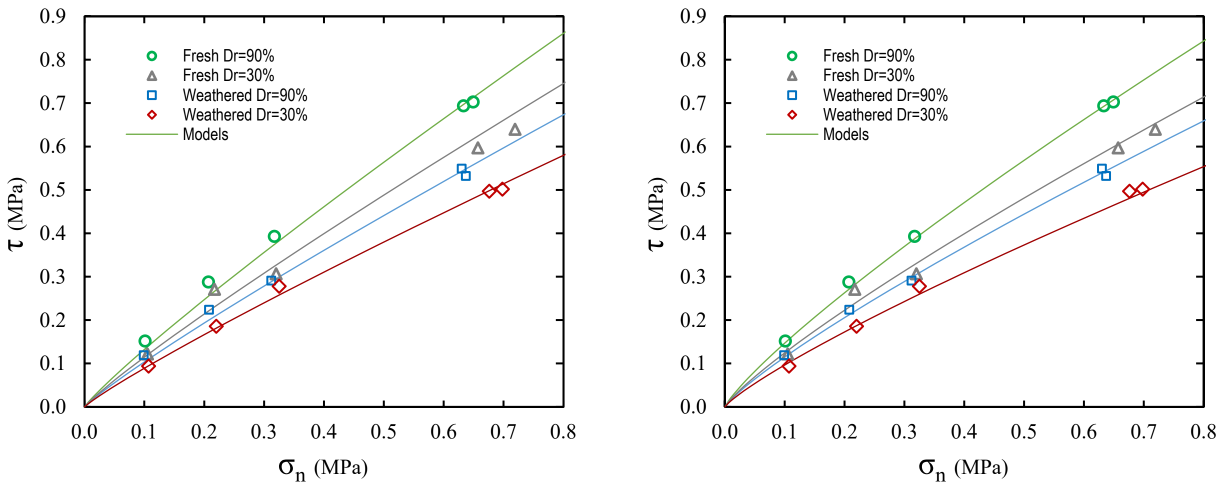

(a) (b)

Figure 10 Test results and model shear strength envelopes for fresh and weathered basalt considering (a) default empirical model parameters and (b) custom-fit model parameters

The proposed rockfill failure criterion and empirical model were evaluated for their ability to predict the strength of the fresh basalt rockfill and to account for strength reductions caused by weathering. Because direct shear testing was performed at multiple normal stresses and void ratios, it was possible to use a generalised strength model accounting for the effects of compaction, rockfill quality and envelope curvature by substituting Equation 10 into Equation 3, resulting in Equation 11.

$$\tau = \tan(\emptyset'_{e=0} - \omega \times e)\,(10\,p_a)^{1-m}\,{\sigma_n}^m \tag{11}$$

First, the recommended default empirical model parameters were applied to the fresh basalt data, as shown in Table 5 (e.g. $\emptyset'_{e=0}$ = 53˚ for basalt, based on Table 2). The effects of weathering were considered by applying a simple reduction of the secant friction angle by $\emptyset'_{reduction}$ = 7˚, resulting in an excellent fit to the observed test data with with R^2 = 0.990. The implementation of the reduction in the secant friction angle is shown in Equation 12.

$$\tau_{weathered} = \tan(\emptyset'_{e=0} - \omega \times e - \emptyset'_{reduction})\,(10\,p_a)^{1-m}\,\sigma_n{}^m \quad (12)$$

where:

$\tau_{weathered}$ = shear stress at failure of weathered rockfill

$\emptyset'_{reduction}$ = reduction in secant friction angle due to weathering.

Table 5 Fitting parameters used to model the fresh and weathered basalt rockfill

Model type	$\boldsymbol{\emptyset'_{e=0}}$	$\boldsymbol{\emptyset'_{reduction}}$	$\boldsymbol{\omega}$	$\boldsymbol{m}$	$\boldsymbol{R^2}$
Default	53°	7°	20°	0.90	0.990
Custom fit	53°	7°	23°	0.84	0.996

Additionally, because extensive testing data were available, the model parameters were optimised to best fit the results, which yielded no change in $\emptyset'_{e=0}$ or $\emptyset'_{reduction}$, but did result in slight adjustments to the parameters ω and m, as detailed in Table 5. This optimisation improved the model fit to R^2 = 0.996. The resulting shear strength models are illustrated in Figure 10.

The proposed failure criterion accurately predicted the strength of the fresh basalt in both dense and loose conditions, and successfully modelled the reduction in strength due to weathering through a simple reduction of the secant friction angle. It is important to emphasise that the reduction in the secant friction angle determined here is specific to the basalt subjected to the particular leachate used in these tests; therefore, calibration of the strength reduction would be necessary for other weathering or leaching scenarios involving different solutions or rock types. Nonetheless, these results demonstrate that the proposed model can effectively account for strength reduction in rockfill due to weathering, making strength adjustments straightforward and easy to interpret by adjusting only the secant friction angle.

5.2 Consolidation of rockfill

Structures built of loosely placed rockfill experience substantial consolidation due to the rearrangement and crushing of particles under their self-weight (Charles 1990; Valenzuela et al. 2008). Volumetric strains exceeding 10% and settlements of more than 10 m have been observed at vertical stress levels near 2 MPa (approx. 100 m in depth) in large rockfill stockpiles (Osses et al. 2024). This consolidation reduces the void ratio and porosity, leading to increased shear strength and stiffness, and reduced permeability. This section extends the empirical model to estimate the increase in rockfill strength due to natural consolidation with depth as a function of the initial compaction state and applied stress.

An oedometer test (i.e. 1D consolidation test) is a laboratory method used to measure how a soil sample compresses when subjected to vertical loading under confined lateral conditions. It provides data to quantify how void ratio changes with vertical effective stress, which can permit estimation of densification with depth in a rockfill stockpile. Oedometer test data on coarse rockfill samples and run-of-mine waste rock (ROM WR) samples with a loose starting condition reported in the literature, in addition to data provided by the authors (Mine #1 data), were compiled in order to develop a model for final void ratio after consolidation (e_f), as shown in Figure 11 and Equation 13. While distinct preconsolidation stress breakpoints are not observed in the data, the samples from the different studies do appear to share a similar primary consolidation line. In addition, data points at low stress values appear to be highly influenced by the degree of compaction performed before testing (i.e the initial void ratio, e_i). The proposed model in Equation 13 is therefore a funcion of the effective vertical stress (σ_v) and e_i.

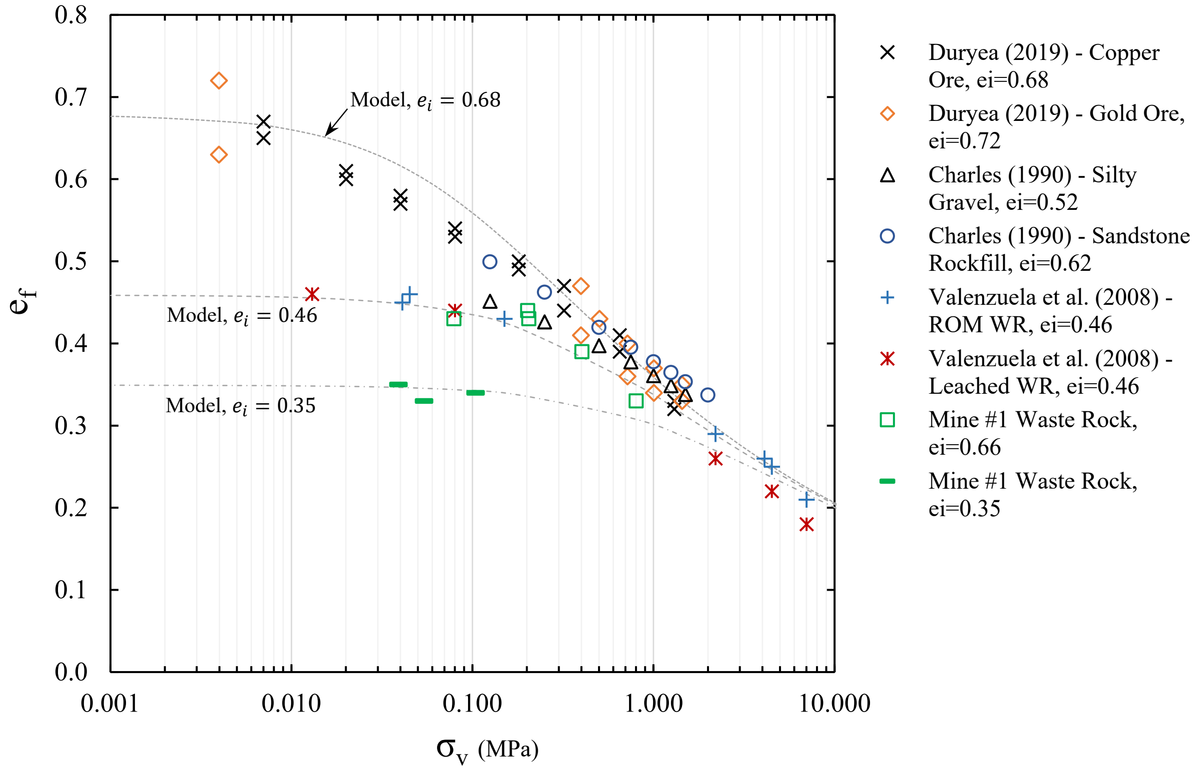

Figure 11 Oedometer tests on coarse rockfill and the proposed model for different initial void ratios

$$e_f = 0.65 \left(\frac{\sigma_v}{p_a} + \frac{0.18}{{e_i}^4}\right)^{-0.25} \tag{13}$$

where:

σ_v = effective vertical stress

e_i = initial void ratio

e_f = final void ratio at the end of the consolidation phase.

This stress-dependent model for e_f can be used directly within the proposed strength framework, since the empirical model estimates the secant friction angle in terms of void ratio. Substituting Equations 10 and 13 into the strength criterion (Equation 4) yields a shear strength model that is based on a stress-dependent void ratio, as shown in Equation 14 (with the simplifying assumption that the consolidation stress is equivalent to the normal stress on the failure plane).

$$\tau = \tan\left(\emptyset'_{e=0} - \omega \times 0.65 \left(\frac{\sigma_n}{p_a} + \frac{0.18}{{e_i}^4}\right)^{-0.25}\right)(10\, p_a)^{0.1}\, {\sigma_n}^{0.9} \tag{14}$$

Figure 12 presents calculated secant friction angles and strength envelopes generated from Equation 14 for low quality rockfill ($\emptyset'_{e=0}$ = 47˚) and various values of e_i. Figure 12a demonstrates that strength gains due to consolidation are highly sensitive to the initial void ratio. At higher stress levels, the envelopes converge, indicating that the influence of initial density diminishes with depth.

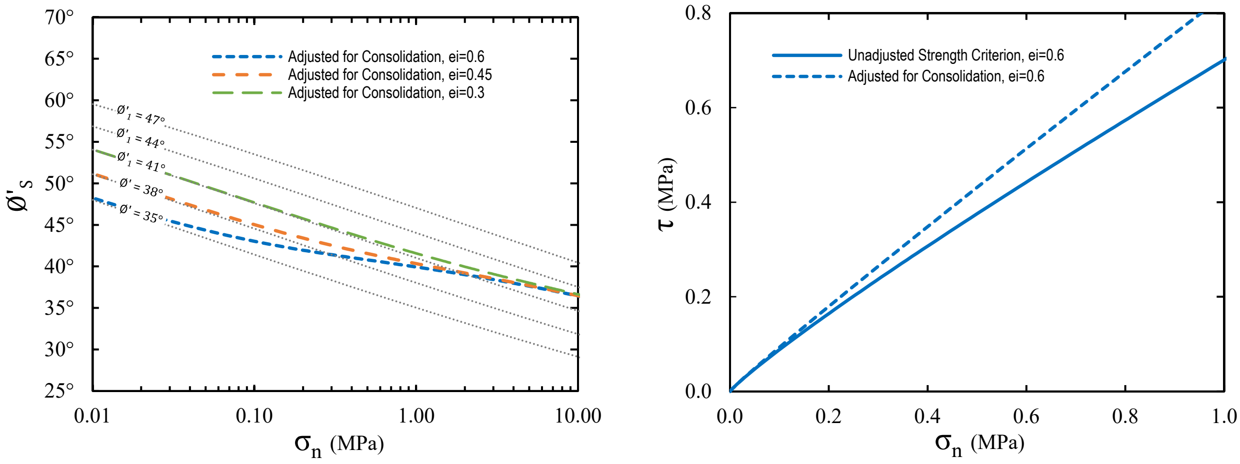

(a) (b)

Figure 12 (a) Secant friction angle for low quality rockfill adjusted for consolidation for various initial void ratios; (b) Shear strength envelope for low quality rockfill adjusted for consolidation, $e_i = 0.6$

5.2.1 Example slope analysis

An as-built slope from a 200 m high active waste dump at a North American gold mine was selected as a case study to evaluate the proposed strength models using 2D limit equilibrium analysis. The facility was constructed by end-dumping waste rock, including siltstone, claystone and sandstone, with typical rock quality designation values ranging from 0 to 20% and an unconfined compressive strength of approximately 30 MPa. A photograph of the active end dump is shown in Figure 13a. Using Table 2 and Equation 10, the estimated nonlinear strength parameters for these materials under loose end-dumped placement conditions are $\emptyset_e'$ = 47˚, e_i = 0.6, and $\emptyset_1'$ = 35˚.

The active end dump was optically scanned to capture the as-built slope profile, as shown in Figure 13b. The dump has an overall slope angle of 37° and exhibits characteristic crest over-steepening with a slope angle of 41° for the upper segment of the slope. The lower portion of the slope has minor runout of coarse material, resulting in a 34° slope angle at the toe. This geometry is typical for high end-dumped waste rock slopes in the authors' experience. No slope instabilities on the waste dump were observed at the site.

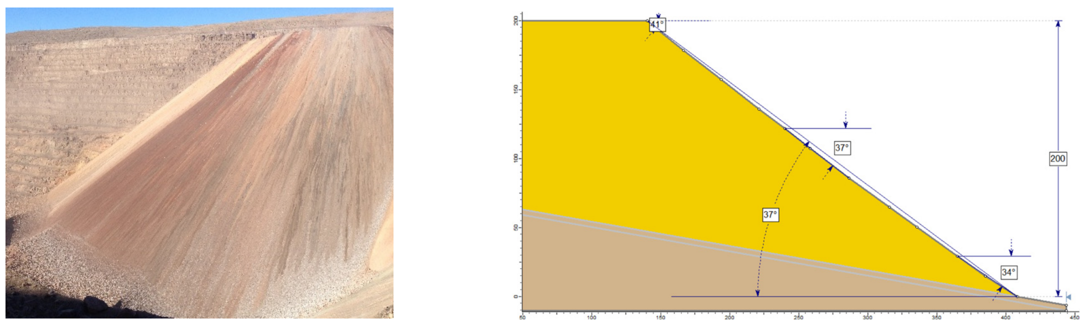

(a) (b)

Figure 13 (a) Photograph of a 200 m high stockpile constructed with end-dumping at the study site; (b) Scanned profile and measured slope angles at the active end dump face of the study site (distances in m)

Stability analysis results for the unadjusted strength criterion (Equation 4) can be seen in Figure 14a and yielded a Factor of Safety (FOS) value of 1.11 for the as-built slope (density of 20 $^{kN}/_{m^3}$, no pore pressure and e_i = 0.6 assumed for all materials). To test deeper optimised shear surfaces at higher stress levels, a second case was analysed that included a weak foundation layer dipping at 10° with no cohesion and a friction angle of 25°. This second case resulted in a minimum FOS = 1.01, as shown in Figure 14b.

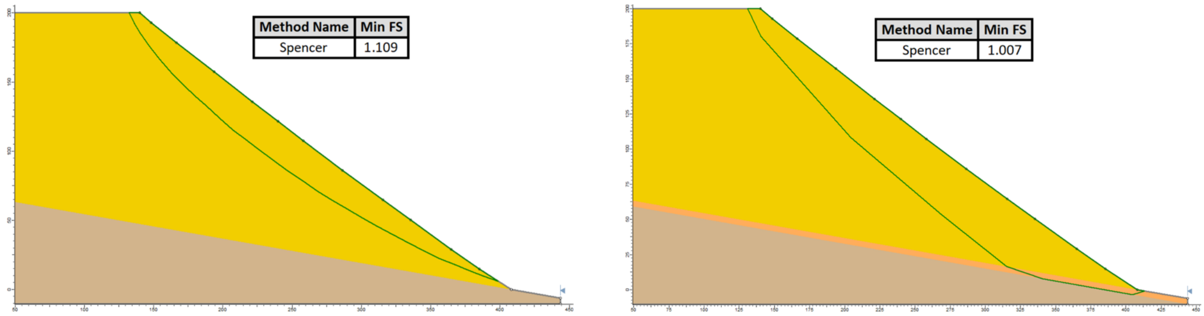

(a) (b)

Figure 14 2D limit equilibrium analysis of low quality/loose rockfill for (a) the stockpile only and (b) the stockpile with a weak foundation layer (distances in m)

The same slope configurations were analysed using Equation 14, accounting for expected consolidation and resulting void ratio decrease with depth. The FOS increased by +0.12 for the base case (Figure 15a) and by +0.09 for the case with the weak foundation layer (Figure 15b), indicating a significant improvement in predicted long-term stability due to consolidation.

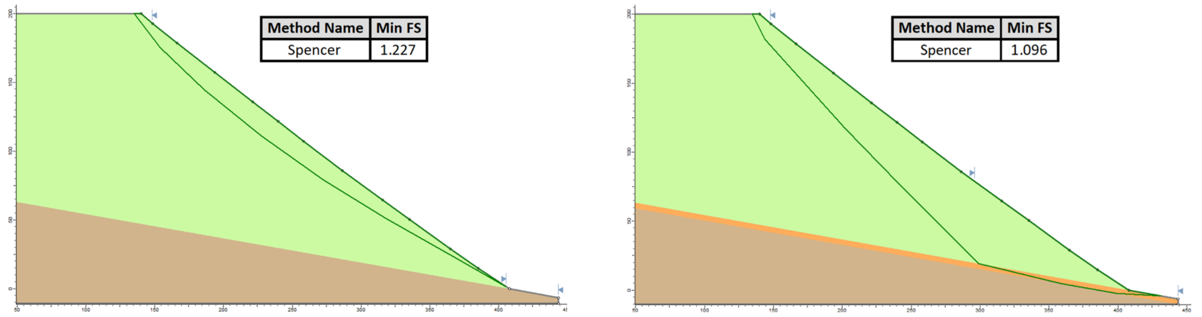

(a) (b)

Figure 15 2D limit equilibrium analysis of low quality/loose rockfill with strength adjustment for consolidation for (a) stockpile only and (b) stockpile with weak foundation layer (distances in m)

Although consolidation can improve rockfill strength over time, the process is slow. Long-term settlement rates have been observed to resemble the secondary compression behaviour of clays (Charles 1990), and full consolidation in large dumps may take many years. Therefore, Equation 14 is not recommended for operational or short-term slope stability assessments. Instead, it may be applied to long-term evaluations such as closure design or for analysis of very old piles.

Additionally, consolidation may result in limited improvement for anisotropic failure mechanisms. If weak layers are formed during construction, consolidation of the surrounding rockfill may not improve stability at the interfaces of those layers. For example, dumping a layer with high fines content near the slope face (Figure 1) can create slope-parallel weak layers. To minimise the potential for such failure modes, best construction practice should therefore avoid placing poor-quality material (e.g. with high fines content) within the outer shell of the final dump geometry.

6 Limitations

The proposed empirical models are intended to guide initial evaluations and should not be considered a complete substitute for site-specific characterisation. They provide a useful basis for preliminary evaluation and should be confirmed during construction and operation with laboratory and field measurements. The gradation thresholds and rock type groupings are intended as guidance ranges rather than strict cutoffs, and conservative assumptions are recommended when materials fall near a boundary unless site data suggest otherwise.

While the database spans a broad range of lithologies, representation is uneven, reducing confidence for less common rock types. For example, quartzite is represented by more than four times as many tests as diorite. The lowest UCS value in the database is 25 MPa, so rockfills composed of weaker particles could perform below model predictions. Testing practices such as downsizing or scalping large particles can also influence results. Partially saturated, undrained, or peak-residual behaviour conditions were not explicitly considered. These limitations highlight that the envelopes should be applied with caution outside the ranges of the database. Site-specific testing remains essential, especially for high-consequence projects where uncertainty in strength predictions cannot be tolerated.

7 Conclusion

This work summarises a practical nonlinear strength criterion and empirical model for rockfill that balances simplicity, accuracy and field applicability. The nonlinear formulation reproduces established strength envelopes, transitions smoothly between material classes, relies on a single intuitive fitting parameter and can be applied using either laboratory or field data. By linking strength to void ratio and rock type, the empirical model enables rapid strength estimation across a wide range of rockfill conditions, even when site data are limited. Two practical applications were demonstrated: strength reduction due to weathering and strength gain from consolidation with depth. Together, the proposed models offer a streamlined and reliable approach to estimating nonlinear rockfill strength, supporting safer and more realistic slope stability assessments.

Acknowledgement

The authors acknowledge the support of Call & Nicholas, Inc, the University of Oulu, WSP, and Piteau Associates.

References

Anyaegbunam, AJ 2015, 'Nonlinear power-type failure laws for geomaterials: Synthesis from triaxial data, properties, and applications', *International Journal of Geomechanics*, vol. 15, no. 1, https://doi.org/10.1061/(ASCE)GM.1943-5622.0000348

Arrieta, M 2025, *Rockfill Test Database*, Zenodo, https://doi.org/10.5281/zenodo.14665504

Bahrani, N & Kaiser, PK 2020, 'Influence of degree of interlock on confined strength of jointed hard rock masses', *Journal of Rock Mechanics and Geotechnical Engineering*, vol. 12, no. 6, pp. 1152–1170, https://doi.org/10.1016/j.jrmge.2020.06.004

Baker, R 2004, 'Nonlinear Mohr envelopes based on triaxial data', *Journal of Geotechnical and Geoenvironmental Engineering*, vol. 130, no. 5, pp. 498–506, https://doi.org/10.1061/(ASCE)1090-0241(2004)130:5(498)

Balmer, G 1952, 'A General Analytical Solution for Mohr's Envelope', *Proceedings of American Society of Test Materials*, vol. 52, American Society for Testing Materials, West Conshohocken, pp. 1260–1271.

Barton, N 2016, 'Nonlinear shear strength for rock, rock joints, rockfill and interfaces', *Innovative Infrastructure Solutions*, vol. 1, no. 30, https://doi.org/10.1007/s41062-016-0011-1

Charles, JA & Watts, KS 1980, 'The influence of confining pressure on the shear strength of compacted rockfill', *Géotechnique*, vol. 30 no. 4, pp. 353–367, https://doi.org/10.1680/geot.1980.30.4.353

Charles, JA 1990, 'Laboratory compression tests and the deformation of rockfill structures', in E Maranha das Neves (ed.), *Advances in Rockfill Structures*, Springer Netherlands, Dordrecht, pp. 73–95.

Cylwik, SD, Arrieta, M, Cunning, J & Hawley, PM 2025, 'Update to the Leps strength envelopes for rockfill based on 900 large-scale triaxial tests', *International Journal of Geomechanics*, vol. 15, no. 12, 04025285, https://doi.org/10.1061/IJGNAI.GMENG-12050

Cylwik, SD, Childs, DW, Mahoney, DM, Plange, KM & Grubb, CM 2024, 'Post-peak multi-stage triaxial testing of miniature rock mass samples', *Proceedings 58th US Rock Mechanics/Geomechanics Symposium*, American Rock Mechanics Association, Westminster, https://doi.org/10.56952/ARMA-2024-1092

Cylwik, SD, Killian, JR & Cicchini, PF 2023, 'A practical nonlinear strength criterion for rock masses and other geological materials', in RE Hammah, S Javankhoshdel, T Yacoub, A Azami & A McQuillan (eds), *Proceedings of the Rocscience International Conference*, Atlantis Press, Dordrecht, pp. 681–699, https://doi.org/10.2991/978-94-6463-258-3_63

Douglas, KJ 2002, *The Shear Strength of Rock Masses*, PhD thesis, University of New South Wales, Sydney.

Duryea, PD 2019, 'Assessment of leach ore dry unit weight and hydraulic performance', *Proceedings of Tailings and Mine Waste 2019*, The University of British Columbia, Vancouver, pp. 953–964.

Hawley, M & Cunning, J 2017, *Guidelines for Mine Waste Dump and Stockpile Design*, CSIRO Publishing, Clayton.

Indraratna, B, Ionescu, D & Christie, HD 1998, 'Shear behavior of railway ballast based on large-scale triaxial tests', *Journal of Geotechnical and Geoenvironmental Engineering,* vol. 124, no. 5, pp. 439–449, https://doi.org/10.1061/(ASCE)1090-0241(1998)124:5(439)

Indraratna, B, Wijewardena, L & Balasubramaniam, A 1993, 'Large-scale triaxial testing of greywacke rockfill', *Géotechnique*, vol. 43, no. 1, pp. 539–543, https://doi.org/10.1680/geot.1994.44.3.539

Ladanyi, B & Archambault, G 1969, 'Simulation of shear behavior of a jointed rock mass', *Proceedings of the 11th US Symposium on Rock Mechanics,* The American Institute of Mining, Metallurgical and Petroleum Engineers, San Ramon.

Leps, TM 1970, 'Review of shearing strength of rockfill', *Journal of the Soil Mechanics and Foundations Division*, vol. 96, no. 4, pp. 1159–1170, https://doi.org/10.1061/JSFEAQ.0001433

Leps, TM 1988, 'Rockfill dam design and analysis', in RB Jansen (ed.), *Advanced Dam Engineering for Design, Construction, and Rehabilitation*, Van Nostrand Reinhold, New York, pp. 368–387, https://doi.org/10.1007/978-1-4613-0857-7_12

Osses, R, Pineda, J, Ovalle, C, Linero, S & Saez, E 2024, 'Scale and suction effects on compressibility and time-dependent deformation of mine waste rock material', *Engineering Geology*, vol. 340, https://doi.org/10.1016/j.enggeo.2024.107668

Ovalle, C, Linero, S, Dano, C, Bard, E, Hicher, PY & Osses, R 2020, 'Data compilation from large drained compression triaxial tests on coarse crushable rockfill materials', *Journal of Geotechnical and Geoenvironmental Engineering*, vol. 146, no. 9, https://doi.org/10.1061/(ASCE)GT.1943-5606.0002314

Park, J & Santamarina, JC 2017, 'Revised soil classification system for coarse-fine mixtures', *Journal of Geotechnical and Geoenvironmental Engineering*, vol. 143, no. 8, https://doi.org/10.1061/(ASCE)GT.1943-5606.0001705

Sayão, AS, Maia, PC & Nunes, ALL 2005, 'Considerations on the shear strength behaviour of weathered rockfill', *Proceedings of the 16th International Conference on Soil Mechanics and Geotechnical Engineering*, IOS Press, Amsterdam, pp. 1917–1920, https://doi.org/10.3233/978-1-61499-656-9-1917

Valenzuela, L, Bard, E, Campaña, J & Anabalón, ME 2008, 'High waste rock dumps — challenges and developments', in AB Fourie (ed.), *Rock Dumps 2008: Proceedings of the First International Seminar on the Management of Rock Dumps, Stockpiles and Heap Leach Pads*, Australian Centre for Geomechanics, Perth, pp. 65–78, https://doi.org/10.36487/ACG_repo/802_6

Xiao, Y, Liu, H, Zhang, W, Liu, H, Yin, F & Wang, Y 2016, 'Testing and modeling of rockfill materials: A review', *Journal of Rock Mechanics and Geotechnical Engineering*, vol. 8, no. 3, pp. 415–422, https://doi.org/10.1016/j.jrmge.2015.09.009

Yu, H, Ng, K, Grana, D, Alvarado, V, Kaszuba, J & Campbell, E 2020, 'A generalized power-law criterion for rocks based on Mohr failure theory', *International Journal of Rock Mechanics and Mining Sciences*, vol. 128, https://doi.org/10.1016/j.ijrmms.2020.104274